RSC Advances

PAPER

View Article Online
View Journal | View Issue

Cite this: *RSC Adv.*, 2021, **11**, 1679

Binding interactions and FRET between bovine serum albumin and various phenothiazine-/anthracene-based dyes: a structure–property relationship†

Shouvik Bhuin,‡ Sayantan Halder,‡ Subit Kumar Saha * and Manab Chakravarty *

The present study demonstrates binding interactions and Förster resonance energy transfer (FRET) between bovine serum albumin (BSA) and a series of structurally and electronically diverse phenothiazine (**PTZ**) and anthracene (**ANT**) dyes. Upon selective excitation of tryptophan (Trp) residues of BSA, radiationless energy transfer to a dye takes place, resulting in fluorescence quenching of the former. Fluorescence quenching mechanisms, FRET parameters, possible locations, and binding constants of dyes with the BSA have been examined to deduce a structure–property relationship. The mechanism of quenching is apparently static in nature. **PTZ** dyes with heteroatoms and a pentyl tail (**C5-PTZ**) attached to them were found to have a stronger binding affinity with BSA as compared to **ANT** dyes. Stronger binding affinities of **C5-PTZ** dyes with BSA result in greater energy transfer efficiencies (E_T). A dye with a strong electron-withdrawing group present in it has shown better energy accepting capability. A FRET study with dicyanoaniline (**DCA**) analogs of **PTZ** and **ANT** dyes (**C5-PTZDCA** and **ANTDCA**, respectively) revealed that E_T depends on electronic and structural factors of molecules. An almost orthogonal geometry between **ANT** and **DCA** moieties (~79°) in **ANTDCA** induces the greater extent of electron transfer from **ANT** to **DCA**, showing a higher E_T for this dye as compared to **C5-PTZDCA** in which the torsion angle is only ~38°. Further, the observed facts have been validated by experimentally determined bandgaps (using cyclic voltammetry experiments) for all the dyes. Thus, the hydrophobic character and the presence of interactive substituents along with the electron-accepting abilities majorly control the FRET for such dyes with BSA.

Received 11th November 2020
Accepted 15th December 2020

DOI: 10.1039/d0ra09580j

rsc.li/rsc-advances

1. Introduction

Serum albumin has been identified as the most abundant protein in plasma. Many researchers remain focused on studying the interactions of bioactive compounds with plasma proteins, mainly serum albumin.[1] Upon binding with the serum albumin, the biological activities may be reduced or enhanced and can provide a transportation path. Bovine Serum Albumin (BSA) is a well-studied protein due to its structural homology with human serum albumin and high abundance. BSA has three structurally distinct domains, I, II, and III, with two subdomains (A and B) in each of the areas.[2] Out of two Trp residues in BSA, Trp-134 is located on the surface of domain I, and Trp-213 is situated in the hydrophobic pocket of domain II. Upon excitation at ~295 nm, the intrinsic fluorescence can be originated selectively from Trp residues of BSA. These Trp residues act as donors in the energy transfer process with an acceptor, and this process can be radiative or non-radiative. Förster or fluorescence resonance energy transfer (FRET) is a radiationless process without emission and reabsorption of photons. Energy exchange takes place between oscillating dipoles of donor and acceptor of similar resonating frequencies.[3] Since the discovery of the FRET, researchers have been actively utilizing this potential non-radiative tool to unveil numerous facts related to the field of supramolecular materials and biomedical research and development.[4,5] There is a rapid growth in the invention of donor–acceptor combinations for the FRET applications. However, constructing an appropriate donor–acceptor pair for the FRET is still a challenge because it needs to meet primary influencing criteria such as distance, spectral overlap, and dipole orientation between donors and acceptors.[6] There are numerous applications where donors and/or acceptors in FRET are used as fluorescence site markers.[7,8] In the present study, a series of phenothiazine and anthracenyl molecules (Chart 1) are examined as acceptors for the energy transfer from the donors *i.e.*, Trp residues of BSA. To our knowledge, both these structural motifs are not tested for FRET

Department of Chemistry, Birla Institute of Technology and Sciences-Pilani, Hyderabad Campuses, Hyderabad-500078, Telangana, India. E-mail: manab@hyderabad.bits-pilani.ac.in; sksaha@hyderabad.bits-pilani.ac.in

† Electronic supplementary information (ESI) available. CCDC 2041739 and 2041742. For ESI and crystallographic data in CIF or other electronic format see DOI: 10.1039/d0ra09580j

‡ Shouvik Bhuin and Sayantan Haldar have Contributed equally.

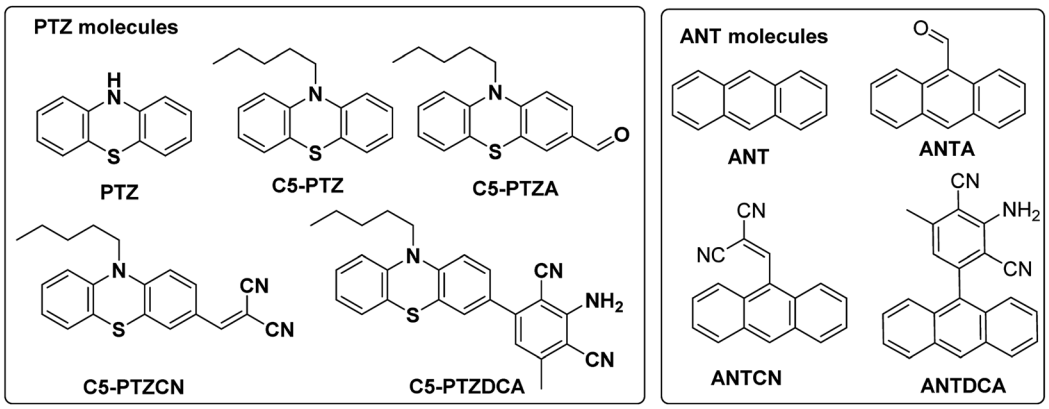

Chart 1 Phenothiazine and anthracenyl molecules that are studied herein for the FRET with BSA.

studies with BSA before. There are a few reports on complicated phenothiazine-linked molecules for metal ion sensing through FRET.[9,10] As benzothiazole type systems are often found to be suitable for FRET,[11,12] the electron-rich phenothiazine core is of our particular interest.

Additionally, the questions arise on the requirement of thia and aza part in a system for an efficient FRET phenomenon. Therefore, we also intend to explore the FRET on anthracenyl-based fluorophores. Notably, anthracene and phenothiazine are not analogous due to the fundamental structural differences; however, we dealt with similar substituents for both the skeletons. Apart from a few known dyes, the dicyanoaniline (DCA) analogs [**PTZDCA** and **ANTDCA**, Chart 1] with acceptor–donor–acceptor (A–D–A) architecture bring special attention to this FRET study.[13,14] Furthermore, the FRET analysis using non-traditional donor–acceptor combinations is very much appealing.[6] Most of these traditional compounds emit at UV-Vis region but with somewhat commendable Stokes shifts compared to the previous report.[6] Intriguingly, the FRET between phenothiazine or anthracene-based molecules and BSA has enabled them to offer as good acceptors. Such acceptors are focused on their convincing applications in the FRET. Mechanistic insights are specified to find quenching of Trp-fluorescence by each of the dyes. An attempt has been made to find the possible relation between the structures of dyes and various properties, such as binding strength/locations and energy transfer efficiency. The governing effect of substituted hydrophobic and electron-withdrawing groups, the position of substitution on the features mentioned above, has also been elucidated.

2. Experimental section

2.1. Materials

The known phenothiazine and anthracene compounds like **C5-PTZ**, **C5-PTZA**, and **ANTCN** were synthesized using reported procedures.[15,16] **C5-PTZCN**, **C5-PTZDCA**, and **ANTDCA** are the compounds that were newly synthesized. Their structures were verified by FT-IR, LCMS (Liquid Chromatography Mass Spectrometry)/HRMS (High-Resolution Mass Spectrometry), and ^{1}H and ^{13}C NMR data (see ESI; pages (3–6) and Fig. (S11–S16)†). **PTZ**, **ANT**, **ANTA**, and **BSA** were procured from Alfa-Aesar and Sigma Aldrich. They were taken into use as received. BSA protein concentration was kept constant at 5 μM for all measurements. HEPES buffer was bought from SRL, India. H_2SO_4 and NaOH were procured from SDFCL, India, and SRL, India, respectively. Quinine sulfate was obtained from Sigma Aldrich. Spectral grade tetrabutylammonium perchlorate (TBAP) and MeCN were purchased from TCI, India.

2.2. Methods

A 10 mM solution of HEPES buffer was prepared with Milli-Q water, and its pH was adjusted to 7.4. H_2SO_4 and NaOH solution was used to adjust the pH of the buffer solution. BSA stock solution was prepared with a freshly prepared buffer solution. Stock solutions of the different dyes (phenothiazine and anthracene series of compounds) were prepared (~0.5 mM each) in pure methanol for recording the UV-vis absorption and fluorescence spectra. All stock solutions were carefully degassed with a pure N_2 gas for 15 minutes before use. For the FRET study between BSA and each individual dye, at a fixed concentration of BSA (5 μM), the concentration of dye was gradually increased in the range of 0 μM −15 μM. The total volume of each solution was kept at 2 mL. A JASCO (model V-650) UV-vis spectrophotometer with a quartz cell of path length 1 cm with a Teflon stopper was used to record the absorption spectra. A FluoroLog-TM (Horiba Scientific) spectrofluorimeter was used for steady-state fluorescence measurements using a quartz cell of path length 1 cm with a Teflon stopper. For fluorescence measurements, all the samples were excited at 295 nm. Slit widths for both excitation and emission were 2.5 nm, that along with the scan rates, were maintained constant for all fluorescence measurements. All the fluorescence spectra were corrected for instrument sensitivity and also to avoid any inner filter effect. Electrochemical assessments were conducted using an Autolab PGSTAT128N potentiostat. Cyclic Voltammetry (CV) of the samples were performed by switching the applied voltage in −3 V to +3 V; using a cleaned glassy carbon (GC) electrode as a working electrode (WE). The Pt-wire and Ag/AgCl were used as a counter electrode (CE) and a reference electrode (RE),

respectively, and a 0.1 M tetrabutylammonium perchlorate (TBAP) in acetonitrile was used as an electrolyte in a typical three-electrode system. A sample solution in acetonitrile was mixed with electrolyte to study the electrochemical behavior of samples. The redox reaction that happened on the surface of GC, were recorded in NOVA 2.1.1. software. HOMO/LUMO energy levels were determined from the onset of oxidation/reduction potentials in the fullness of positive/negative scans. A Jasco-J 1500 CD spectropolarimeter was utilized for recording the far – UV circular dichroism (CD) spectra of appropriate systems in the wavelength range of 190–260 nm. A cuvette having path length as 0.1 cm was used. Each CD spectrum was recorded at a scan speed of 50 nm min^{-1} with a spectral bandwidth of 2.5 nm. The spectra obtained for different BSA systems were subtracted by buffer spectra for background correction. All measurements were performed at 298.15 ± 1 K temperature.

3. Results and discussions

An electron-rich and inexpensive phenothiazine core is picked up for the FRET-study with BSA, based on the earlier reports on related thiazole as a well-established motif for FRET applications.[9,17] However, the presence of pyridyl nitrogen (electron-withdrawing sp^2-hydridized) in the thiazole type molecules displays the primary difference between phenothiazine and benzothiazole cores. To investigate beyond the conventional donor–acceptor systems, DCA was installed with the **C5PTZ** core to afford **C5PTZDCA** as an acceptor to elucidate the electronic factor in the FRET process. For the comparative study with a similar tricyclic electron-rich system, anthracene is coupled with the DCA motif to afford **ANTDCA**. Thus, we investigate the scope of changes in FRET with the same trend of functionalities in these two different scaffolds.

3.1. Synthesis of the compounds

C5-PTZDCA compound was synthesized newly *via* a one-pot reaction of aldehyde and malononitrile in the presence of triethylamine (TEA) as depicted in Scheme 1. In the first step, the requirement of the base was not mandatory just because of the highly active methylene group. The dicyano compound, **C5-PTZCN** was not isolated separately herein. Instead, the addition of excess malononitrile and TEA directly produced penta-substituted benzene, **C5-PTZDCA**, in 63% yield. Thus, this strategy is somewhat different than the existing one,[18] hitherto reported.

The compound **ANTDCA** was synthesized in a manner similar to **C5-PTZDCA** with a 25% yield, possibly due to the various reaction scopes with anthracenyl core. A solvent-free twisted path[19] was also adopted to afford **ANTDCA**, but the result was not pleasing.

All the synthesized compounds are characterized by NMR, HRMS/LCMS, and FT-IR spectroscopy (see ESI† for details). Mostly, the molecular structure for new compounds **C5-**

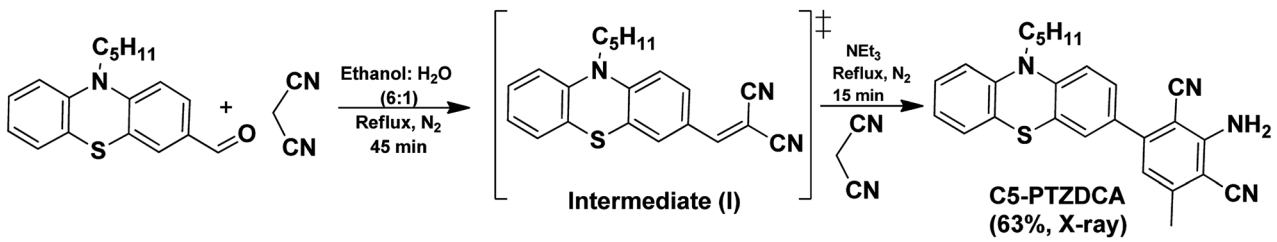

Scheme 1 Synthesis of C5-PTZDCA.

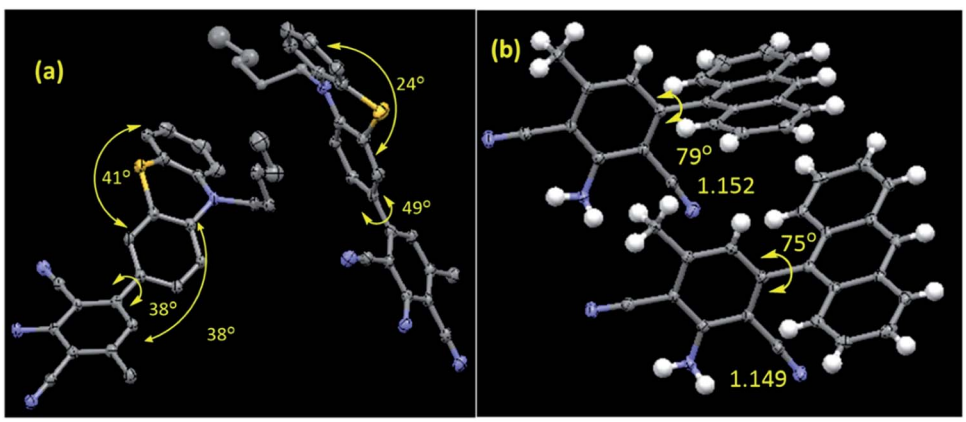

Fig. 1 The molecular structures of (a) C5-PTZDCA and (b) ANTDCA. The selected torsion angles (°) and bond lengths (Å) are also given. There are two molecules in one asymmetric unit for both the systems. Hydrogens are omitted for the C5-PTZDCA for clarity. CCDC Number: ANTDCA 2041742; C5-PTZDCA: 2041739.

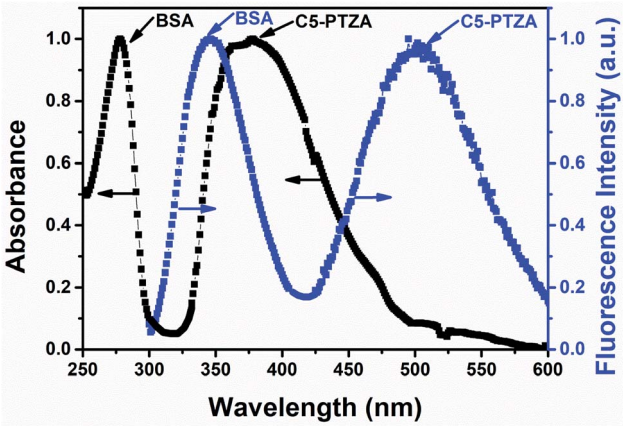

Fig. 2 Normalized absorption and fluorescence spectra of 5 μM BSA in the presence of 5 μM **C5-PTZA** in an aqueous HEPES buffer solution. λ_{ex} for fluorescence measurements is 295 nm.

PTZDCA and **ANTDCA** are determined unequivocally with the help of single-crystal X-ray diffraction studies (Fig. 1). The X-ray structures help to identify the exact position of cyano, amine, and methyl groups within the dicyanoaniline (DCA) ring. Moreover, the torsion angle between the DCA and anthracene or phenothiazine could also be measured as depicted in Fig. 1.

3.2. Systematic absorption and fluorescence measurements to study FRET

In this investigation, the FRET behavior between BSA and all the organic dyes has been demonstrated by carrying out systematic absorption and fluorescence measurements. The detailed on FRET are discussed in the ESI.† Before we deal in a sequence, let us demonstrate the representative plot of FRET with one of the above-listed compounds **C5-PTZA** (Fig. 2) to elucidate the process. The normalized absorption and fluorescence spectra of 5 μM BSA solution were recorded in the presence of an extrinsic fluorophore **C5-PTZA** (5 μM) in an aqueous HEPES buffer solution. The peak maximum of the more extended wavelength absorption band of BSA is located at 279 nm, while the absorption peak maximum of **C5-PTZA** appeared at 373 nm.

Upon excitation of the sample (a mixture of BSA and **C5-PTZA**) with a light of 295 nm, two fluorescence bands at 347 nm and 502 nm were found due to the emissions from both BSA and **C5-PTZA**, respectively. Still, the emission from **C5-PTZA** is unexpected using λ_{ex} = 295 nm. Albeit, a significant extent of overlap between the fluorescence band of BSA and absorption band of **C5-PTZA** (Fig. 2) along with the fluorescence from both the species indicate a definite possibility of FRET occurring between them. Among various intrinsic fluorophores as part of the origin of BSA's fluorescence, we have focused explicitly on to excite only Trp residues to avoid the fluorescence contribution from the other amino acid residues of BSA such as phenylalanine (Phe) and tyrosine (Tyr). That is why the excitation wavelength of 295 nm has been selectively preferred.[20] Further, between two Trp residues in BSA, Trp-134 resides in the hydrophilic environment, whereas Trp-213 chooses a relatively less polar part of BSA.[21] Intriguingly, such FRET behavior was experienced with all the dyes used herein except molecular anthracene (**ANT**).

To understand the origin of fluorescence quenching for Trp residues of BSA, the radiative rate constant (k_r) of this emission process is a vital parameter and calculated using Strickler–Berg equation (eqn (1)) considering no solvent interactions and change in the excited-state geometry:[22–24]

$$k_r = 3.13 \times 10^{-9} \bar{\upsilon}_0^2 \int \varepsilon d\bar{\upsilon} \simeq \bar{\upsilon}_0^2 f \quad (1)$$

where $\bar{\upsilon}_0$ represents the wavenumber when the absorption of the BSA is maximum, ε is the extinction coefficient, and f denotes the oscillator strength. The absorption spectra of BSA in the absence and presence of each molecule (excluding **ANT**) as quenchers were recorded to calculate k_r and f values in each case and tabulated in Table 1.

Notably, the change in radiative rate constants of the BSA in the presence or absence of a dye is not impressive. The changes in the oscillator strength fall within the range of 0.01–4.61%, which has an almost negligible contribution to the observed quenching (29.0–66.9%, Table 1). Therefore, the fluorescence quenching of BSA by the molecules confirms the involvement of the energy transfer process to a greater extent.

Next, the fluorescence quenching of Trp residues in BSA was studied at different concentrations for each of the dyes, individually except for **ANT**. This study has enabled us to explain the mechanism of quenching, binding efficiency with the protein, and location in the protein. Fluorescence quenching using

Table 1 The radiative rate constant (k_r), % change in oscillator strength (f), and % quenching of fluorescence from Trp residues of BSA

Quencher (dye)	$k_r \times 10^{-10}$ (without dye) (s^{-1})	$k_r \times 10^{-10}$ (with dye) (s^{-1})	% change in f	% quenching
PTZ	1.45	1.45	0.01	31.7
C5-PTZ	1.45	1.49	3.81	34.9
C5-PTZA	1.45	1.51	4.61	66.9
C5-PTZCN	1.45	1.46	0.11	49.6
C5-PTZDCA	1.45	1.49	3.87	29.0
ANTA	1.45	1.42	2.93	34.9
ANTCN	1.45	1.42	2.26	30.7
ANTDCA	1.45	1.41	3.30	35.8

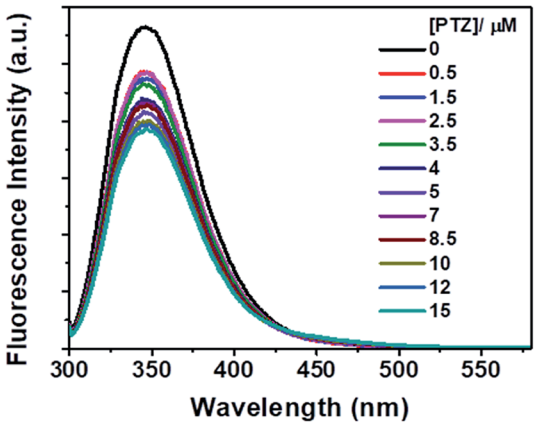

Fig. 3 Fluorescence spectra of Trp residues of BSA in the presence of different concentrations of **PTZ**. [BSA] = 5 μM. λ_{ex} = 295 nm.

these molecules and analysis of quenching data in each case has been attempted to decipher the observed facts.

3.2.1 FRET between BSA and phenothiazinyl compounds. As intended, the series of molecules with phenothiazine (**PTZ**) core (Chart 1; Fig. 1a) were initially studied. Upon incremental addition of **PTZ** at a fixed concentration of BSA (5 μM), there was a diminution in the fluorescence intensity of BSA, which can be ascribed to the energy transfer from Trp residues to **PTZ**.

However, no increase in the fluorescence intensity of **PTZ** could be found, being a non-fluorescent dye (Fig. 3). The above-mentioned calculated values (Table 1) of the radiative rate constants (k_r)/oscillator strength (f) and the analysis of data have confirmed the energy transfer as a cause for the fluorescence quenching. The FRET efficiency depends on donor–acceptor proximity and spectral overlap, not necessarily that the acceptor should be fluorescent.[25] There are recent reports on the use of several non-fluorescent acceptors/quenchers, *e.g.*, Dabcyl,[26–28] the black hole quenchers, BHQ,[28–30] QSY-7, and BHQ2,[28] and QSY-9,[31] different nucleotides,[28] Guanosine,[32,33] and Au nanoparticles.[27,34] The development of non-fluorescent dye derivatives-based FRET assays is a promising area that can lead to broad applications in the receptor field.[25] A relationship between fluorescence quenching and concentration of quencher is represented by the Stern–Volmer (S–V) equation,[35] (eqn (2)):

$$\frac{F_o}{F} = 1 + K_{SV}[Q] = 1 + k_q\tau_o[Q] \quad (2)$$

where F_o and F are the fluorescence intensities of Trp residues of BSA in the absence and presence of a quencher, respectively; K_{SV}, k_q, and τ_o represent S–V quenching constant, bimolecular quenching rate constant, and the average lifetime of the fluorophore in absence of a quencher, respectively. The fluorescence quenching of Trp residues is analyzed using the S–V plot, as displayed in Fig. 4a. The observed downward curvature of the S–V plot indicates the fractional accessibilities of two different Trp residues of BSA to **PTZ**.[35] The downward curvature in protein fluorescence quenching generally occurs in the presence of a polar or charged quencher.[35] Being polar/charged, the quencher cannot penetrate the hydrophobic interior of the protein. Here, the parent compound **PTZ** thus shows differing accessibility to the Trp residues. There is no significant change in the peak maxima of BSA with an increase in the concentration of **PTZ**. The S–V plot has been modified (Fig. 4b) based on eqn S(1) in Note S1 in ESI† to find the fraction of Trp residues accessible to **PTZ** (f_a in eqn S(2)).†[35]

The correlation coefficient of the linear fitting of the modified S–V plot (Fig. 4b) is found to be 0.9997. The calculated f_a and K_a values from the intercept and the slope of the modified S–V plot are found to be 0.43 and 1.92×10^5 M^{-1}, respectively. So, 43% of Trp residues in BSA are only accessible to **PTZ**. The estimated S–V quenching constant of an accessible fraction ($K_a = k_q\tau_o$) is 1.92×10^5 M^{-1}. Considering the τ_o for BSA: $\sim 10^{-8}$ s (ref. 35–37) the bimolecular quenching rate constant, k_q appears as 1.92×10^{13} M^{-1} s^{-1}. However, the maximum value of k_q for a diffusion-controlled quenching process with a biopolymer is $\sim 2.0 \times 10^{10}$ M^{-1} s^{-1}.[3] It implies that the mechanism of the quenching of available fraction is static. By assuming the same and independent binding sites for BSA in case of a static quenching, the binding constant K' and the number of binding sites (n) have been calculated based on eqn S(3) in Note S2.†[38]

Fig. S1† displays the plot of $\log[(F_o - F)/F]$ *versus* $\log(1/([\mathbf{PTZ}] - (F_o - F)[BSA]/F_o))$. The number of binding sites, n, and the binding constant, K' calculated from the slope and intercept,

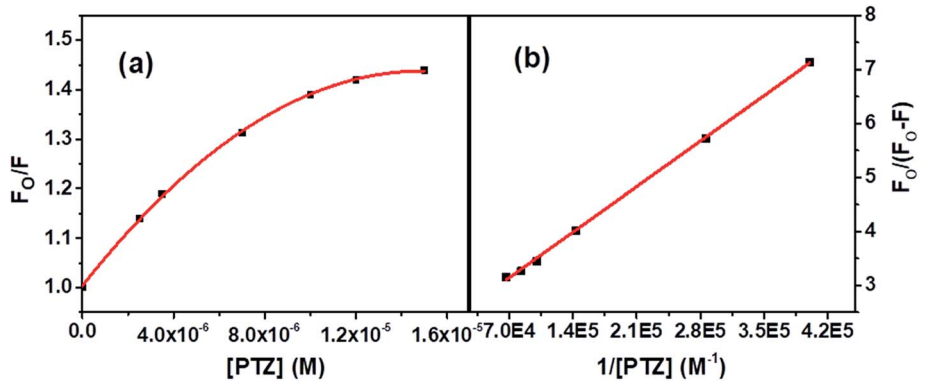

Fig. 4 (a) S–V plot for quenching of the Trp fluorescence by **PTZ** in BSA, and (b) modified S–V plot for quenching the Trp fluorescence by **PTZ** in BSA. [BSA] = 5 μM. λ_{ex} = 295 nm.

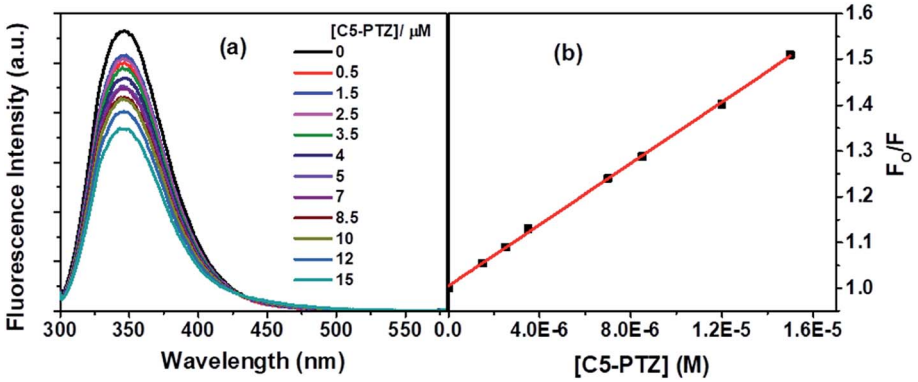

Fig. 5 (a) Fluorescence spectra of Trp residues of BSA with increasing concentration of C5 PTZ, and (b) S–V plot for quenching of the Trp fluorescence by C5-PTZ. [BSA] = 5 μM. λ_{ex} = 295 nm.

respectively of the linear fitting [R^2 = 0.9997] of the data are found to be 0.35 and 6.19 × 10^3 M^{-1}, respectively.

Next, we dealt with the **C5-PTZ**, possibly more hydrophobic, as compared to **PTZ** due to the introduction of the pentyl chain. Notably, **C5-PTZ** is also non-fluorescent like **PTZ**. The parameters listed in Table 1 support the energy transfer as a reason for fluorescence quenching of Trp residues in the presence of **C5-PTZ** as a quencher. Fluorescence spectra of Trp residues of BSA at different concentrations of **C5-PTZ** are shown by Fig. 5a, and Fig. 5b displays the change in fluorescence intensity with increasing concentration of **C5-PTZ** based on eqn (2). The observed linear S–V plot (R^2 = 0.9995) indicates both the Trp residues are equally accessible to the dye, **C5-PTZ**. Unlike **PTZ**, **C5-PTZ** with a pentyl tail in the molecule can penetrate the protein and bind to a comparatively interior site, and that facilitates equal accessibility of both the Trp residues.

The S–V constant, K_{SV} (= $k_q\tau_o$) calculated from the linear fitting of the quenching data (Fig. 5b) is found to be 3.35 × 10^4 M^{-1}. Taking $\tau_o = 10^{-8}$ s, the k_q is calculated to be 3.35 × 10^{12} M^{-1} s^{-1}. As the k_q value lies beyond the diffusion-controlled limit, thus it is a static quenching. The binding constant (K') and the number of binding sites, n calculated after linear fitting [Fig. S2,† R^2 = 0.9997] of the quenching data based on eqn S(3),† are found to be 2.46 × 10^4 M^{-1} and 0.73, respectively. The higher binding constant of **C5-PTZ** than that for **PTZ** specifies the binding of the former at the more hydrophobic site of the BSA. Thus, the presence of a hydrocarbon tail enables the dye binding to a comparatively more hydrophobic site.[39]

The next dye, **C5-PTZA**, with aldehyde functionality (Chart 1), is found to be highly fluorescent, unlike **PTZ** and **C5-PTZ**. Upon excitation at 295 nm, the fluorescence from both Trp residues of BSA and **C5-PTZA** have been recorded at different concentrations of the latter, and the corresponding fluorescence spectra with an isoemissive point at 445 nm are shown by Fig. 6a.

Fig. 6a illustrates a gradual decrease in the fluorescence intensity of the Trp residues (donor) of BSA with a concomitant increase in the fluorescence intensity of **C5-PTZA** (as an acceptor) through the FRET process with increasing concentration of **C5-PTZA**. This trend is well displayed in Fig. 6b, which shows the rise and fall in F/F_o of the acceptor and the donor, respectively. Detailed scrutiny revealed that the peak maximum of Trp fluorescence is blue-shifted from 347 nm to 344 nm upon the increasing concentration of **C5-PTZA** within the range of 0 μM to 15 μM. There could be two possible reasons for it. First, the shift of peak maximum to a shorter wavelength with increasing **C5-PTZA** concentration could be due to the fact that the Trp fluorescence at a longer wavelength is getting quenched more readily than that at a shorter wavelength.[35] Trp-134 being

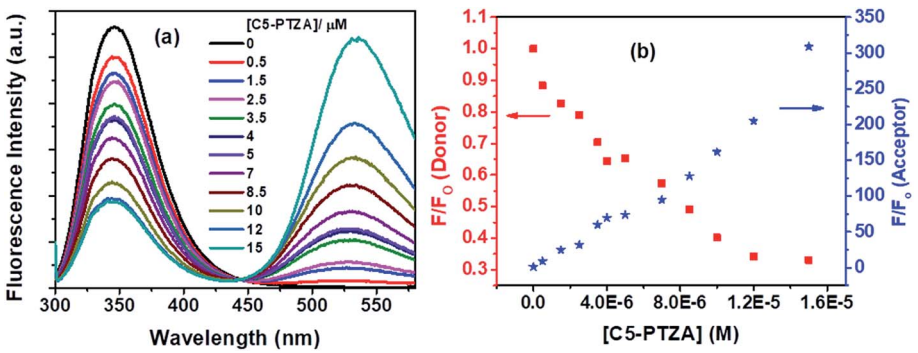

Fig. 6 (a) Fluorescence spectra of Trp residues of BSA and C5-PTZA at varying concentrations of C5-PTZA, and (b) decrement in fluorescence intensity of donor (Trp in BSA) with concomitant enhancement in fluorescence intensity of acceptor (C5-PTZA) with increasing concentration of C5-PTZA in the FRET process. [BSA] = 5 μM. λ_{ex} = 295 nm.

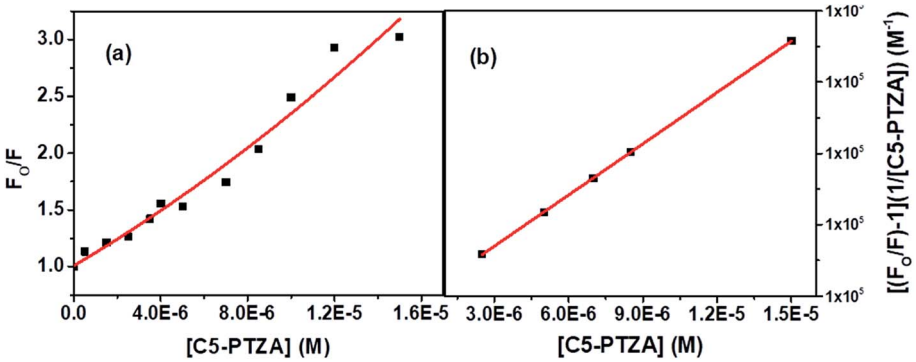

Fig. 7 (a) S–V plot for quenching of the Trp fluorescence by **C5-PTZA** in BSA, and (b) modified S–V plot for quenching of the Trp fluorescence by **C5-PTZA** in BSA. [BSA] = 5 μM. λ_{ex} = 295 nm.

present in a comparatively hydrophilic environment should have fluorescence at a relatively longer wavelength as compared to Trp-213. Thus as compared to Trp-213, Trp-134 is more accessible to **C5-PTZA**. Secondly, it could also be due to the changes in secondary structure of BSA in presence of a dye. To verify it, the circular dichroism spectra for BSA in presence of different concentrations of C5-PTZA have been recorded and given as Fig S3.† The % α-helix of the native BSA is found to be changed from 62.7% to 55.4%.

The S–V plot, in this case, exhibits an upward curvature, concave towards the *y*-axis at higher concentrations of the quencher (**C5-PTZA**) (Fig. 7a). This trend can be well described by using concurrent static and dynamic quenching mechanisms.[35] The modified S–V equation for a quenching process through both static and dynamic quenching can be written as eqn S(4) in Note S3.† which can be further modified through eqn S(5) and S(6).†

Fig. 7b presents the modified S–V plot ($R^2 = 0.9999$) based on eqn S(6).† Then, by solving the quadratic equation, we get the values of the S–V dynamic quenching constant (K_D) as 5.96 × 10^4 M^{-1} and the S–V static quenching constant (K_S) as 4.02 × 10^4 M^{-1}. Assuming that eqn S(3)† is applicable in this case as static quenching is in place, the binding constant (K') and the number of binding sites (n) calculated from the linear fitting (Fig. S4,† $R^2 = 0.9999$) of the data based on eqn S(3)† are found to be 1.30 × 10^5 M^{-1} and 1.06, respectively. The higher value of binding constant for **C5-PTZA** as compared to **C5-PTZ** infers that –CHO functionality in **C5-PTZA** induces added binding interactions with the protein.

Subsequently, another dye, **C5-PTZCN** (Chart 1), has been used with much higher electron-accepting capability due to the presence of di-cyano functionality linked through a π-bond. Fig. 8a shows changes in fluorescence spectra of both donor and acceptor parts with increasing concentration of **C5-PTZCN** with an isoemissive point at ~447 nm. Like the previous dye, **C5-PTZA**, a gradual diminution in the fluorescence intensity of the Trp residues of BSA with a simultaneous rise in the fluorescence intensity of **C5-PTZCN** are presented in Fig. 8b.

The blue shift in the fluorescence peak maximum of BSA is due to the same reason, as discussed in the case of **C5-PTZA**. The S–V plot for this quenching of fluorescence presents a downward curvature (Fig. 9a). The modified S–V plot based on eqn S(1)† is shown in Fig. 9b ($R^2 = 0.9999$).

The fractional accessibility of the dye to the Trp residues of BSA indicated by the downward curvature in the S–V plot leads us to calculate f_a and K_a from the intercept and the slope of the plot in Fig. 9b based on eqn S(1)†. The f_a and K_a values are estimated to be 0.87 and 2.06 × 10^5 M^{-1}, respectively. So, 87%

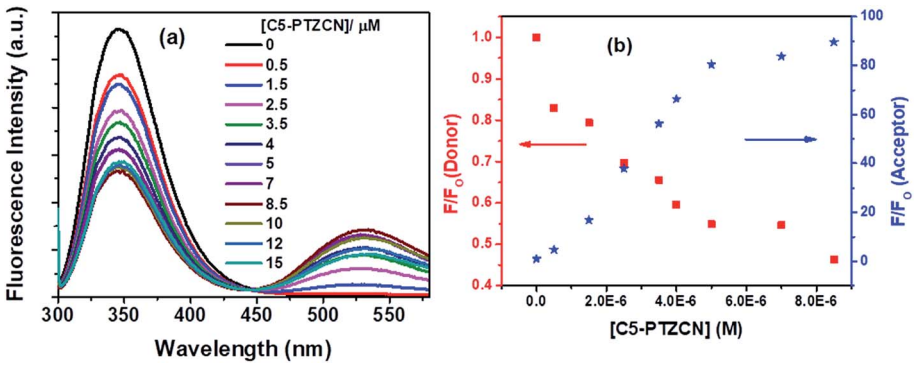

Fig. 8 (a) Fluorescence spectra of Trp residues of BSA and **C5-PTZCN** with increasing concentration of the dye, and (b) decrement in fluorescence intensity of donor (Trp residues in BSA) with concomitant enhancement in fluorescence intensity of acceptor (**C5-PTZCN**) with increasing concentration of **C5-PTZCN** in the FRET process. [BSA] = 5 μM. λ_{ex} = 295 nm.

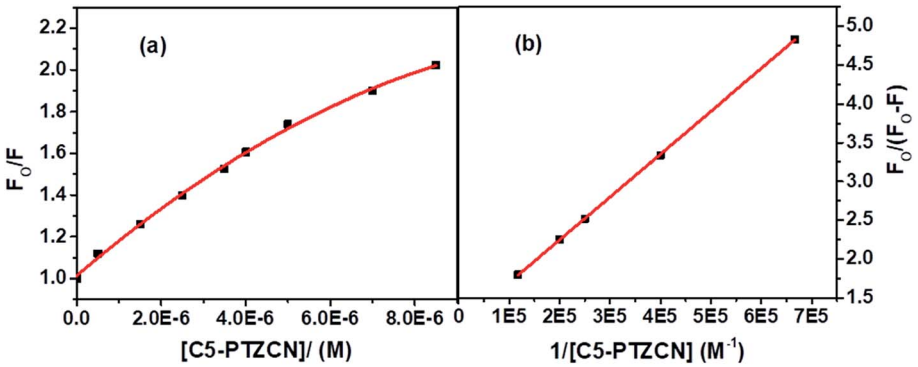

Fig. 9 (a) S–V plot for quenching of Trp fluorescence by **C5-PTZCN** in BSA, and (b) modified S–V plot for quenching of the Trp fluorescence by **C5-PTZCN** in BSA. [BSA] = 5 μM. λ_{ex} = 295 nm.

of Trp residues of BSA are accessible to the **C5-PTZCN**. The bimolecular quenching constant, $k_q = 2.06 \times 10^5\ M^{-1}/10^{-8}\ s = 2.06 \times 10^{13}\ M^{-1}\ s^{-1}$, which is beyond the diffusion-controlled limit. Thus, the mechanism of quenching appears to be static. The binding constant (K') and the number of binding sites (n) calculated from the linear fitting (Fig. S5,† $R^2 = 0.9999$) of the quenching data based on eqn S(3)† are found to be $1.21 \times 10^5\ M^{-1}$ and 0.63, respectively. Of note, the binding of **C5-PTZCN** is almost the same as that of **C5-PTZA.**

Besides, the new dye studied in this series is **C5-PTZDCA** (Chart 1), dicyanoaniline (DCA) moiety attached to the **C5-PTZ** core. Fig. 10a shows the fluorescence spectra of donor–acceptor pair with increasing concentration of the acceptor, **C5-PTZDCA**, with an isoemissive point at ~403 nm. The dye, **C5-PTZDCA**, with a strong acceptor–donor–acceptor unit along with a methyl group, is found to be highly fluorescent. The gradual decrease in the fluorescence intensity of the Trp residues of BSA with a simultaneous rise in the fluorescence intensity of **C5-PTZDCA** is represented by Fig. 10b. The blue-shift in the emission peak maximum of BSA indicating fractional accessibility of Trp residues and/or changes in secondary structure of BSA is noted in this case as well.

The S–V plot for this system also displayed a slight downward curvature (Fig. 11a). The modified S–V plot (Fig. 11b) based on eqn S(1)† was scrutinized ($R^2 = 0.9965$) to find the fractional accessibility (f_a), as well as the S–V quenching constant (K_a) those, are found out to be 0.85 and $3.59 \times 10^4\ M^{-1}$. So, 85% of Trp residues of BSA are accessible to the **C5-PTZDCA.** The quenching rate constant, k_q is found to be $3.59 \times 10^{12}\ M^{-1}\ s^{-1}$, reflecting the static quenching mechanism. The respective values of binding constant (K') and a number of binding sites (n) calculated from the linear fitting of the data in Fig. S6† ($R^2 = 0.9999$) based on eqn S(5)† are calculated to be $2.81 \times 10^5\ M^{-1}$ and 0.97.

3.2.2 FRET between BSA and anthracenyl compounds. Similar studies, as discussed above, have also been carried out with an anthracenyl series of molecules given in Chart 1. At the very beginning, we took a representative example of FRET using the **ANTA** molecule. Electron-rich molecular anthracene, **ANT**, does not act as an acceptor in the FRET process with BSA as a donor. However, each of its derivatives in the series, such as **ANTA**, **ANTCN**, and **ANTDCA** with significant electron-withdrawing substituents, has shown the FRET phenomenon as an acceptor. In each case, the energy transfer is responsible for the fluorescence quenching of Trp residues of BSA, as supported by data given in Table 1.

Fluorescence quenching of Trp residues by **ANTA** (a weak fluorescent molecule) through the FRET process has been

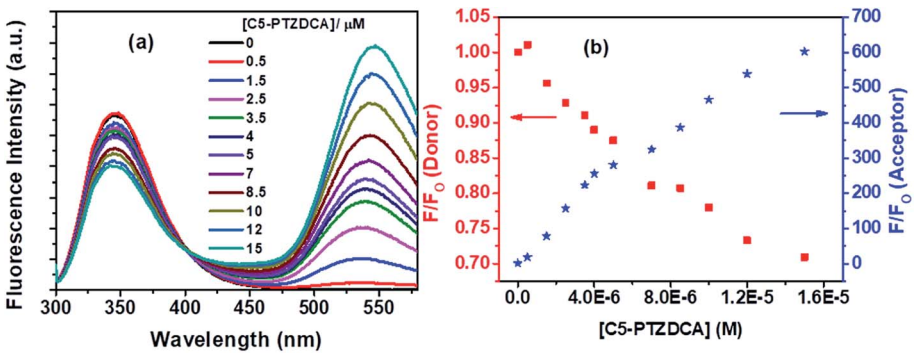

Fig. 10 (a) Fluorescence spectra of Trp residues of BSA and **C5-PTZDCA** with increasing concentration of the dye, and (b) dropping in fluorescence intensity of donor (Trp in BSA) with concomitant enhancement in fluorescence intensity of acceptor (**C5-PTZDCA**) with increasing concentration of **C5-PTZDCA** in the FRET process. [BSA] = 5 μM. λ_{ex} = 295 nm.

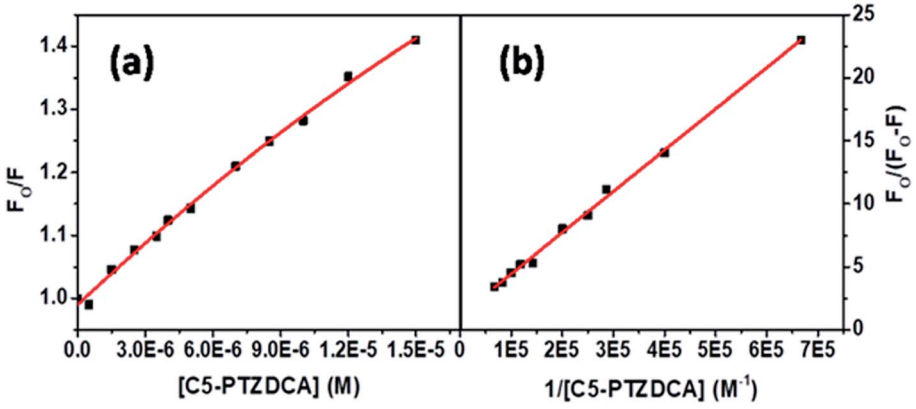

Fig. 11 (a) S–V plot for quenching of the Trp fluorescence by **C5-PTZDCA** in BSA, and (b) modified S–V plot for quenching of the Trp fluorescence by **C5-PTZDCA** in BSA. [BSA] = 5 μM. λ_{ex} = 295 nm.

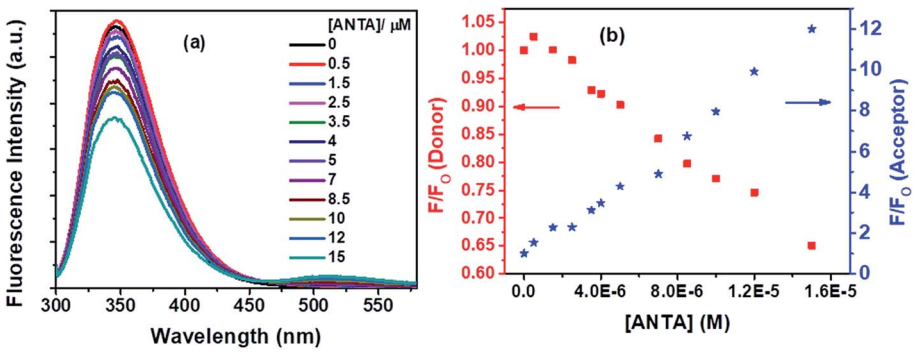

Fig. 12 (a) Fluorescence spectra of Trp residues of BSA and **ANTA** with increasing concentration of **ANTA**, and (b) decrement in fluorescence intensity of donor (Trp residues in BSA) with concomitant enhancement in fluorescence intensity of acceptor (**ANTA**) with increasing concentration of **ANTA** in the FRET process. [BSA] = 5 μM. λ_{ex} = 295 nm.

shown in Fig. 12a. On the gradual treatment of **ANTA**, the fluorescence intensity for Trp residues of BSA is decreased with an increase in fluorescence intensity of **ANTA**, showing an iso-emissive point at ~462 nm (Fig. 12a).

An upward curvature noted in the S–V plot (Fig. 13a) indicates either a combined dynamic and static mechanism of quenching or static quenching with the sphere-of-action (Perrin) model. Based on a modified S–V equation (eqn (S6)†) applicable for concurrent static and dynamic quenching mechanism, the quenching data were plotted. Still, we failed to fit the data to the said equation. It led us to follow the sphere-of-action model as an alternate mechanism of the static part of quenching. The modified S–V equation for the sphere-of-action model is written as eqn S(7) in Note S4.†[35] Further modification done has been shown through eqn S(8) to S(10) and has been discussed in Note S4.†[40]

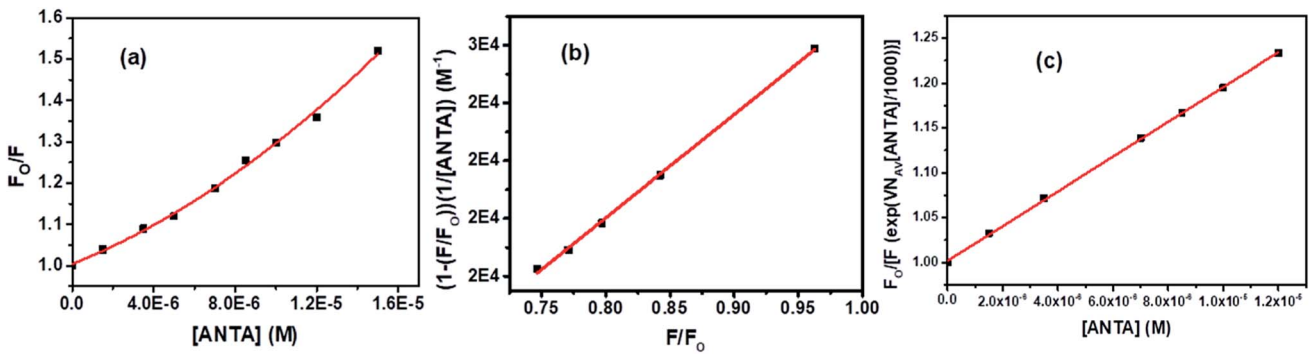

Fig. 13 (a) S–V plot for quenching of Trp fluorescence of BSA by **ANTA**, (b) plot of $(1-(F/F_o))/$[**ANTA**] *versus* F/F_o, and (c) modified S–V plot for quenching of the Trp fluorescence of BSA by **ANTA**. [BSA] = 5 μM. λ_{ex} = 295 nm.

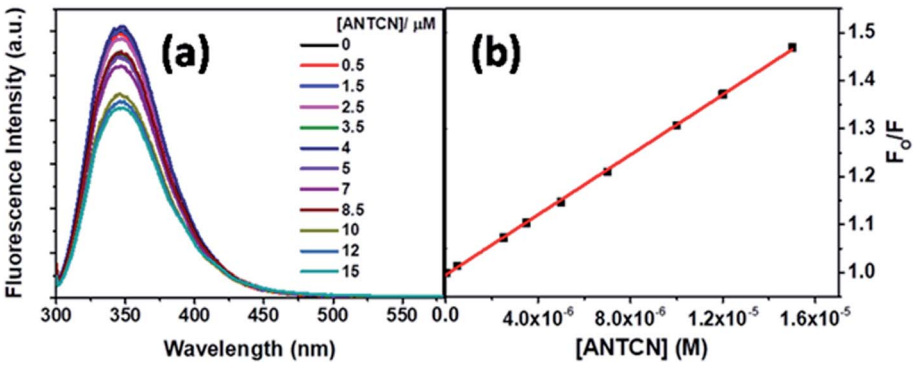

Fig. 14 (a) Fluorescence spectra of Trp residues of BSA and **ANTCN** with increasing concentration of **ANTCN**, and (b) S–V plot for quenching of Trp fluorescence of BSA by **ANTCN**. [BSA] = 5 μM, λ_{ex} = 295 nm.

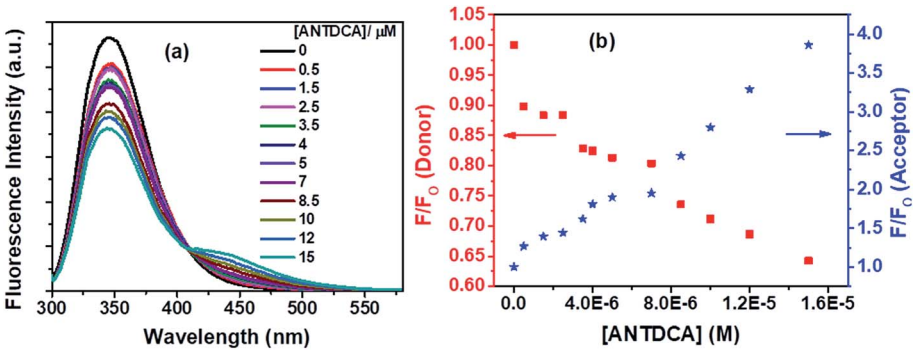

Fig. 15 (a) Fluorescence spectra of Trp residues in BSA with increasing concentration of **ANTDCA**., and (b) lowering in fluorescence intensity of donor (Trp in BSA) with concomitant enhancement in fluorescence intensity of acceptor (**ANTDCA**) with increasing concentration of **ANTDCA** in the FRET process. [BSA] = 5 μM. λ_{ex} = 295 nm.

Based on eqn S(10),† the values of K_D and V have been calculated from the slope and intercept, respectively by linear fitting ($R^2 = 0.9988$) of the data in the plot of $(1 - (F/F_o))/[\mathbf{ANTA}]$ *versus* F/F_o shown by Fig. 13b. The values of K_D and V are found to be 1.79×10^4 M^{-1} and 1.27×10^{-17} liters, respectively. The radius of the sphere of action is calculated to be 144 nm. After calculating the approximate value of V with an assumption of the low value of the term, $VN_{AV}[\mathbf{ANTA}]/1000$ in eqn S(8),† the quenching data have been plotted based on the actual S–V equation for the sphere-of-action model (eqn S(7)†) and shown by Fig. 13c. The S–V dynamic quenching constant was calculated from the slope of the linear fitting ($R^2 = 0.9996$) of the data in the plot of $F_o/F(e^{VN_{AV}[\mathbf{ANTA}]/1000})$ *versus* [**ANTA**] based on eqn S(7).† The K_D value is found to be 1.94×10^4 M^{-1}, which is different from that calculated from the plot in Fig. 13b because of the assumption involved in the derivation of corresponding

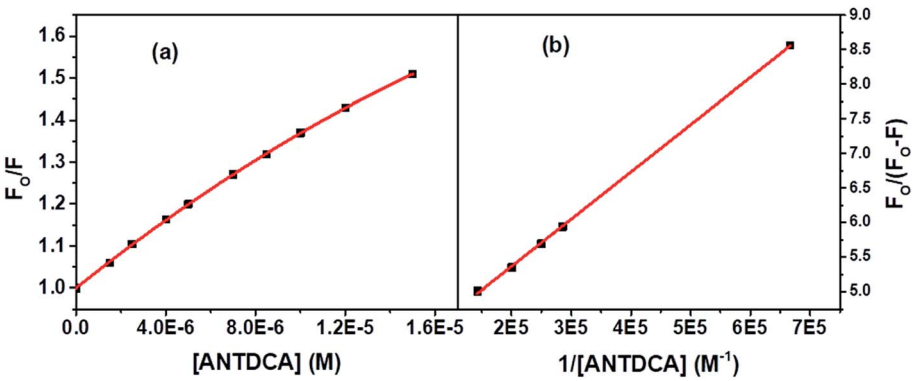

Fig. 16 (a) S–V plot for quenching of the Trp fluorescence in BSA by **ANTDCA**, and (b) modified S–V based on eqn S(3).† [BSA] = 5 μM, λ_{ex} = 295 nm.

Table 2 FRET parameters calculated for the energy transfer process between donor Trp residues of BSA and different dyes as acceptors. Band gap values obtained from CV measurements, λ_{abs}^{max} and λ_{fl}^{max} calculated from UV absorption and fluorescence spectra, respectively for pure dyes and dyes in presence of BSA

Molecules	Overlap Intergral, $(J(\lambda)) \times 10^{-14}$ (M^{-1} cm^{-1} $(nm)^4$)	E_T	R_o (Å)	r (Å)	Band gap (eV)	λ_{abs}^{max} (nm) (without BSA)	λ_{abs}^{max} (nm) (with BSA)	λ_{fl}^{max} (nm) (without BSA)[b]	λ_{fl}^{max} (nm) (with BSA)[c]
PTZ	3.89	0.26	25.1	29.8	5.34	312	326	N.F.[a]	N.F.
C5-PTZ	2.88	0.20	23.9	30.2	5.44	310	325	N.F.	N.F.
C5-PTZA	9.98	0.35	29.4	32.6	4.54	373	398	503	533
C5-PTZCN	7.41	0.45	27.9	28.8	4.37	377	397	497	531
C5-PTZDCA	4.52	0.12	25.7	35.6	4.95	358	374	472	543
ANTA	3.17	0.10	24.3	35.2	4.72	371	404	518	512
ANTCN	4.22	0.11	25.4	36.4	4.67	383	391	N.F.	N.F.
ANTDCA	3.13	0.19	24.2	30.9	4.50	387	390	495	437

[a] NF: non-fluorescent. [b] λ_{ex} = respective absorption peak maximum. [c] λ_{ex} = 295 nm.

eqn S(10).† Assuming that the fraction of molecules presents within the sphere of action at the time of excitation is non-fluorescent and undergoing static fluorescence quenching, eqn S(3)† has been used to calculate the binding constant (K') and the number of binding sites (n) upon linear fitting of the data in Fig. S7† ($R^2 = 0.9999$). The values of K' and n are found to be 3.95×10^4 M^{-1} and 1.31.

Next, **ANTCN** with conjugated dicyano substituents is also non-fluorescent. The fluorescence from Trp residues of BSA in the presence of different concentrations of **ANTCN** is shown in Fig. 14a. The radiative rate constant (k_r) and oscillator strength (f) of the donor in the absence and presence of **ANTCN** and % quenching data given in Table 1 support the energy transfers as a cause for the quenching of Trp fluorescence. It has been discussed above that energy transfer is possible even if the acceptor is non-fluorescent. A linear S–V plot ($R^2 = 0.9995$) for the Trp fluorescence quenching is obtained and displayed in Fig. 14b. The value of S–V quenching constant, K_{SV} calculated from the slope of the plot is found to be 3.13×10^4 M^{-1}, with a corresponding fluorescence quenching rate constant (k_q) value as 3.13×10^{12} M^{-1} s^{-1}. A k_q value beyond the diffusion-controlled limit denotes the static quenching mechanism. The binding constant (K') of **ANTCN** with BSA and the number of binding sites (n) have been calculated from the linear fitting ($R^2 = 0.9999$) of the data in Fig. S8 based on eqn S(3)† and the values are found to be 3.15×10^4 M^{-1} and 1.10, respectively. Thus, the binding constant of **ANTCN** is very close to that of **ANTA**, as noticed in the case of **C5-PTZ** analogs.

With our interest in studying a new electron-rich donor–acceptor–donor (D–A–D) molecular system, **ANTDCA** molecule is considered here for the FRET with BSA. There is a considerable amount of FRET with an isoemissive point at ~409 nm (Fig. 15a). The blue-shift in the emission spectrum of Trp residues of BSA is also observed as discussed above. A trend of decrease in the fluorescence intensity of Trp residues of BSA and an increase of the fluorescence intensity of the dye, **ANTDCA**, are represented by Fig. 15b.

Based on the quenching of the BSA–Trp fluorescence by **ANTDCA**, the S–V plot is identified with slight downward curvature (Fig. 16a). Therefore, quenching data have plotted based on modified S–V eqn S(1)† and are shown by Fig. 16b ($R^2 = 0.9997$). The values of fractional accessibility (f_a) and the S–V quenching constant (K_a) are calculated to be 0.25 and 5.85×10^5 M^{-1}, respectively. So, 25% of Trp residues in BSA are only accessible to the quencher, **ANTDCA**. The quenching rate constant (k_q) is found to be 5.85×10^{13} M^{-1} s^{-1}, indicating a static quenching mechanism. The binding constant (K') and a number of binding sites (n) are found to be 2.38×10^4 M^{-1} and 0.63, respectively [calculated from the linear fitting (Fig. S9,† $R^2 = 0.9998$) of the data based on eqn S(3)].†

3.2.3 FRET parameters. The Förster's distance (R_o), the efficiency of energy transfer (E_T) and the distance (r) between an acceptor quencher dye and donor Trp residues of BSA have been calculated to create a quantitative analysis of FRET between Trp residues of BSA and different dyes.[36] Details of calculation of these parameter along with the calculation of the overlap integral, $J(\lambda)$ have been given in ESI as Note S5.† It is pertinent to

Table 3 Summary of data on nature of S–V plots, quenching mechanisms, quenching constants (K_D/K_S), fractional accessibility (f), binding constant (K'), and number of binding sites (n)

Molecules	Nature of S–V plot	Mechanism of quenching	S–V dynamic quenching constant, K_D (M^{-1})	S–V static quenching constant, K_S (M^{-1})	Bimolecular quenching rate constant (k_q) (M^{-1} s^{-1})	Fractional accessibility of quencher (f)	Binding constant, K' (M^{-1})	No. of binding sites (n)
PTZ	Downward curvature	Static	—	1.92×10^5	1.92×10^{13}	0.43	6.19×10^3	0.35
C5-PTZ	Linear	Static	—	3.35×10^4	3.35×10^{12}	1.00	2.46×10^4	0.73
C5-PTZA	Upward curvature	Both static and dynamic	5.96×10^4	4.02×10^4	—	—	1.30×10^5	1.06
C5-PTZCN	Downward curvature	Static	—	2.06×10^5	2.06×10^{13}	0.87	1.21×10^5	0.63
C5-PTZDCA	Downward curvature	Static	—	3.59×10^4	3.59×10^{12}	0.85	2.81×10^5	0.97
ANTA	Upward curvature	Sphere of action model	1.94×10^4	—	—	—	3.95×10^4	1.31
ANTCN	Linear	Static	—	3.13×10^4	3.13×10^{12}	1.00	3.15×10^4	1.10
ANTDCA	Downward curvature	Static	—	5.85×10^5	5.85×10^{13}	0.25	2.38×10^4	0.63

note that the presence of the two donor moieties needs the assumption of an average distance between donors and acceptors.[3] Also, even though the donor is covalently attached to the protein, but the acceptor dyes are not. However, the high binding constant of each dye with the BSA reduces the possibility of any high uncertainty allowing us to estimate the average distance between a donor and an acceptor. It is noteworthy that all FRET calculations have been done with a ratio of concentration of a dye to BSA of 1 : 1 taking 5 μM concentration of each. With this concentration of each of the donors and the acceptors, the intensity ratios, [$Int_{acceptor}/Int_{donor}$] are found to vary from 0.05 to 0.72. Lowest intensity ratio is found in case of ANTA. However, its relative quantum yield is calculated to be 0.08 which is not very low so that it could contribute a significant error in calculations. The intensity ratios mentioned above are increased with increasing concentration of a dye further reducing the chances of errors in the quenching data.

The overlap between the corrected fluorescence spectrum of Trp residues of BSA as donor and absorption spectrum of **C5-PTZA** as acceptor has been shown as a representative one in Fig. 2. Similar overlapping has also been noted in cases of all other dyes for which overlap integral values have been calculated.

The calculated FRET parameters are given in a tabular form in Table 2. The R_o values measured are in the range of 24.2–29.4 Å, which corroborates well with the range (20–90 Å) for FRET to occur.[3] Thus, the data reflect that dyes are binding close to the Trp residues of BSA. In addition, the band gaps for all dyes have been calculated based on the data obtained from CV experiments to compare the E_T values of the dyes in phenothiazine and anthracenyl series (see Fig. S10† for details). To further support the band gaps data, the absorption peak maxima (λ_{abs}^{max}) of all dyes have been determined. The band gaps and λ_{abs}^{max} values along with λ_{fl}^{max} values are also tabulated in Table 2.

In order to have an overall discussion on the quenching mechanism, energy transfer processes with different dyes as an acceptor, and binding affinities of dyes with the BSA, the quenching data are compiled in Table 3. Few FRET parameters and band gap data tabulated in Table 2 have been used. It can be seen that the quenching mechanism is apparently static. In phenothiazine series, combined static and dynamic quenching has been noted only in the case of **C5-PTZA**. Surprisingly, a combined quenching mechanism has been shown only by **ANTA** among all dyes in anthracenyl series following a sphere of action model of the static part of quenching in this case. Thus, –CHO functionality has some connection with the combined quenching mechanism, possibly because of the interaction between the –CHO group and some active functional group of amino acids of BSA, such as the –NH functionality of Trp residues. The binding affinities of dyes in phenothiazine series are stronger than the corresponding dyes in anthracenyl series could be due to the presence of pentyl tail as well as hetero atoms inducing a greater extent of hydrophobic as well as hydrogen bonding and coulombic attractive interactions in the former than that in the latter. A higher binding constant value of **C5-PTZ** as compared to **PTZ** is due to the presence of a pentyl tail that enhances the hydrophobicity in the former. Among all dyes, including phenothiazine and anthracenyl series, the

energy transfer efficiency, E_T is found to be maximum in the case of **C5-PTZCN** ($E_T = 0.45$), proving itself as the most efficient FRET acceptor with a distance of 28.8 Å from the donor, which is minimum among all other donor–acceptor distances. The next dye which shows E_T closest to **C5-PTZCN** is **C5-PTZA**, with an E_T of 0.35. The binding constants for **C5-PTZCN** and **C5-PTZA** with BSA are found to be very much comparable with the value of 1.21×10^5 and 1.30×10^5 M^{-1}, respectively. Different substituents present in these two dyes must be responsible for the difference in E_T. The presence of more potent electron-withdrawing functionalities (two –CN groups) for **C5-PTZCN** facilitates the compound to be a more efficient acceptor in comparison to **C5-PTZA** that carries one electron-withdrawing –CHO group. The presence of an electron-withdrawing cyano-ester group in a molecule makes it an efficient acceptor, which has been reported by Vijayakumar *et al.*[41] In phenothiazine series, the lowest E_T is observed for **C5-PTZDCA** ($E_T = 0.12$) though it has got the highest binding constant with BSA ($K' = 2.81 \times 10^5$ M^{-1}). A high value of the binding constant of this dye and high accessibility (85%) of Trp residues to this dye imply that the dye binds to the interior of the protein, perhaps with a drive of additional hydrophobic interaction due to the presence of a benzene ring and hydrogen bonding and coulombic interactions with the BSA as a result of the presence of different functional groups such as $–NH_2$ and –CN. However, the lowest E_T for this dye can be attributed to the attachment of electron-donating groups such as amine and methyl that can significantly enrich the electron density to the molecule and hamper the accepting ability of cyanobenzene.[42] Also, the reason due to the presence of acceptor moiety, cyano benzene at a distant position as compared to other dyes cannot be ruled out. This is further supported by the longest r (=35.6 Å, Table 2) in this case. It indicates that the phenothiazine ring with pentyl tail is aligned towards the protein's hydrophobic interior, and the substituted benzene ring is protruded towards the outer hydrophilic site. Moreover, the molecular structure depicts that the dicyanoaniline part is tilted with ~38° torsion angle with folded (~41° folded middle ring) phenothiazine core (Fig. 1). On the other hand, **C5-PTZCN** without any such DCA ring present in the structure shows maximum E_T, and almost the same accessibility (87%) as that is found for **C5-PTZDCA** that offers the shortest average distance (28.8 Å) from the Trp residues of BSA. The lack of electron-withdrawing substituents for **PTZ** and **C5-PTZ** compounds can attribute to lower E_T as compared to **C5-PTZA** and **C5-PTZCN**. Quenching data also dictate that the binding constants for **PTZ** and **C5-PTZ** are comparatively lower than the other three dyes in this series. So, the functional groups present in the other three dyes feasibly undergo some kind of binding interactions with the protein. To check whether the E_T has any relation with the band gap of a dye, the band gap values of all dyes have been calculated (Table 2) from CV measurements (Fig. S10† displays CV diagrams for pure dyes). The increasing E_T order for the dyes of phenothiazine series (Table 2) is found with the following trend: **C5-PTZDCA** < **C5-PTZ** < **PTZ** < **C5-PTZA** < **C5-PTZCN**. However, the decreasing order of band gap is as follows (Table 2): **C5-PTZ** > **PTZ** > **C5-PTZDCA** > **C5-PTZA** > **C5-PTZCN**. With decreasing band gap, we also noticed the expected trend [**C5-PTZ** < **PTZ** < **C5-PTZDCA** < **C5-PTZA** < **C5-PTZCN**] in the increase of λ_{abs}^{max} of pure dyes. The increase in E_T with decreasing the band gap except for **C5-PTZDCA** can be described with the molecular structural factor, dominating over the electronic factor.

As far as anthracenyl series are concerned, their binding affinities with BSA are lower than that for dyes in phenothiazine series as described above. Due to the absence of pentyl tail in anthracenyl series of dyes, they probably bind to the comparatively less hydrophobic/interior sites of the protein. That is why the average distances between the donor and each of dyes, **ANTA** (35.2 Å) and **ANTCN** (36.4 Å) are longer than the corresponding above-mentioned analogs, **C5-PTZA** (32.6 Å) and **C5-PTZCN** (28.8 Å), with eventually smaller E_T values (Table 2). While the respective E_T for **C5-PTZA** and **C5-PTZCN** are 0.35 and 0.45, the E_T for **ANTA** and **ANTCN** are only 0.10 and 0.11, respectively. Now, if we compare between the other two new dyes, **C5-PTZDCA** and **ANTDCA**, the fact that the binding constant of **ANTDCA** is almost one-tenth of that of **C5-PTZDCA**, the former one binds at the comparatively less hydrophobic region, and as a result, its fractional accessibility to the Trp residues is lesser than that of the latter one. However, interestingly the E_T of **ANTDCA** is higher than that of **C5-PTZDCA**, and it can be deciphered by the difference in electronic and structural factors between these two systems. Anthracene is a flat polyaromatic hydrocarbon without any heteroatoms, whereas phenothiazine is a middle ring folded electron-rich core with two specific electron donor atoms such as nitrogen and sulfur. In our recent research, phenothiazine appears to be more electron-rich compared to anthracene.[43] From the molecular structure (Fig. 1), the torsion angle between ANT ring and DCA ring is measured to be ~79°, whereas the torsion angle between the C5-PTZ ring and DCA ring is only ~38°. Thus, a greater extent of charge transfer in **ANTDCA** might be favorable for it to be a better acceptor than **C5-PTZDCA** resulting in a higher E_T in FRET.[44] Moreover, as the DCA is attached to the C5 carbon of **ANTDCA** rather than the C2 carbon of **C5-PTZDCA**, the former one remains closer to the donor in BSA ($r = 30.9$) as compared to the latter ($r = 35.6$). The increasing order of E_T of dyes in anthracenyl series is found to be as follows: **ANTA** < **ANTCN** < **ANTDCA** (Table 2), which is correlated agreeably with the decreasing order of band gaps (Table 2) *i.e.* **ANTA** > **ANTCN** > **ANTDCA** while the increasing order of λ_{abs}^{max} of pure dyes is established as (Table 2): **ANTA** < **ANTCN** < **ANTDCA**. In contrast to **C5-PTZDCA**, **ANTDCA** shows the anticipated energy transfer efficiency from the order of band gap values in anthracenyl series. It depicts that the electronic factor for **ANTDCA** plays an important role.

From the results of fractional accessibilities to the four dyes, **PTZ**, **C5-PTZCN**, **C5-PTZDCA**, and **ANTDCA**, it can be seen that the % accessibilities are high and almost same for **C5-PTZCN** and **C5-PTZDCA**, 87% and 85%, respectively. Thus these two dyes bind to a site from where both the Trp residues are quite accessible. The binding sites must be in the hydrophobic region; otherwise, Trp-213 would not be accessible. For the other two dyes, **PTZ** and **ANTDCA** fractional accessibilities are only 43% and 25%, respectively. Therefore, they bind to

hydrophilic sites. Thus, hydrophobic substitution on dyes makes them more accessible to the Trp residues present in a hydrophobic pocket. Earlier, Karukstis *et al.*[44] also noted the higher fraction of accessibility of Chlorophyll fluorescence by hydrophobic substitution of naphthoquinones. Linear S–V plot obtained in each case of **C5-PTZ** and **ANTCN** is indicative of their binding sites in the protein from where both the Trp residues are equally accessible.

It is to be noted that the fluorescence quenching of BSA as described above is a result of energy transfer from the donor to the acceptor as supported by the data in Table 1 and accordingly the FRET parameters have been estimated. However, as a strategy, the variable mechanisms of quenching in presence of different dyes as quenchers as noted after a detailed analysis of the quenching data have been described.

4. Conclusions

A few easily accessible, structurally and electronically diverse anthracene and phenothiazine dyes are explored for binding-studies with BSA. FRET between Trp residues of BSA and the dyes, mechanism of fluorescence quenching, and their possible locations are examined to deduce a structure–property relationship. The binding efficiency of phenothiazine dyes with a pentyl tail is stronger than that of anthracenyl dyes due to the presence of a hydrocarbon tail and also hetero atoms in the former inducing hydrophobic as well as hydrogen bonding and coulombic attractive interactions. Energy transfer between Trp residues of BSA as a donor and each dye as an acceptor is found to be responsible for fluorescence quenching. Energy transfer has been noted even in cases of non-fluorescent acceptors, **PTZ**, **C5-PTZ**, and **ANTCN**. The mechanism of quenching is static. Concurrent static and dynamic mechanisms have been distinguished only in cases of **C5-PTZA** and **ANTA** with a sphere of action model of the static part of quenching for the latter dye. Dyes with a hydrophobic entity (pentyl tail herein) present in their structures bind with the hydrophobic sites of protein, showing better energy acceptors. Although the binding constant is more significant for **C5-PTZDCA** than **ANTDCA**, the favored energy transfer for **ANTDCA** could be due to its relatively higher electron-transfer capabilities within the molecules and lower acceptor–donor distances. The band gap values of all the dyes are also very much supportive of the observed behavior. Thus, the hydrophobic character and the presence of interactive substituents along with the electron-accepting abilities majorly control the FRET for such acceptor molecules with BSA.

Conflicts of interest

The authors declare no conflict of interest.

Acknowledgements

SB and MC thank CSIR 02(-0289)/17/EMR-II for the financial assistance. The authors thank Susmita Roy, PhD Research Scholar, Department of Chemistry, BITS Pilani, Hyderabad campus, for helping in the CV analysis. CAL lab facilities available at BITS-Pilani Hyderabad is acknowledged.

References

1 J. Tong, T. Hu, A. Qin, J. Z. Sun and B. Z. Tang, Deciphering the binding behaviours of BSA using ionic AIE-active fluorescent probes, *Faraday Discuss.*, 2017, **196**, 285–303.
2 P. Das, A. Mallick, B. Haldar, A. Chakrabarty and N. Chattopadhyay, Fluorescence resonance energy transfer from tryptophan in human serum albumin to a bioactive indoloquinolizine system, *J. Chem. Sci.*, 2007, **119**, 77–82.
3 J. R. Lakowicz, Chapter 13 – Energy Transfer, *Princ. Fluoresc. Spectrosc.*, 2006, pp. 443–475.
4 Z. Dong, Y. Bi, H. Cui, Y. Wang, C. Wang, Y. Li, H. Jin and C. Wang, AIE Supramolecular Assembly with FRET Effect for Visualizing Drug Delivery, *ACS Appl. Mater. Interfaces*, 2019, **11**, 23840–23847.
5 P. B. Jones, B. J. Bacskai and B. T. Hyman, *Chapter 11 Biomedical FRET-FLIM applications*, Elesvier B. V., 1st edn, 2009, vol. 33.
6 K. E. Sapsford, L. Berti and I. L. Medintz, Materials for fluorescence resonance energy transfer analysis: beyond traditional donor–acceptor combinations, *Angew. Chem., Int. Ed.*, 2006, **45**, 4562–4589.
7 R. B. Sekar and A. Periasamy, Fluorescence resonance energy transfer (FRET) microscopy imaging of live cell protein localizations, *J. Cell Biol.*, 2003, **160**, 629–633.
8 L. Wu, C. Huang, B. P. Emery, A. C. Sedgwick, S. D. Bull, X. P. He, H. Tian, J. Yoon, J. L. Sessler and T. D. James, Förster resonance energy transfer (FRET)-based small-molecule sensors and imaging agents, *Chem. Soc. Rev.*, 2020, **49**, 5110–5139.
9 V. Anand, B. Sadhasivam and R. Dhamodharan, Facile synthesis of triphenylamine and phenothiazine-based Schiff bases for aggregation-induced enhanced emission, white light generation, and highly selective and sensitive copper(II) sensing, *New J. Chem.*, 2018, **42**, 18979–18990.
10 K. M. Vengaian, C. D. Britto, K. Sekar, G. Sivaraman and S. Singaravadivel, Phenothiazine-diaminomalenonitrile based Colorimetric and Fluorescence 'turn-off-on' Sensing of Hg^{2+} and S2-, *Sens. Actuators, B*, 2016, **235**, 232–240.
11 K. Rajasekhar, N. Narayanaswamy, N. A. Murugan, G. Kuang, H. Ågren and T. Govindaraju, A High Affinity Red Fluorescence and Colorimetric Probe for Amyloid β Aggregates, *Sci. Rep.*, 2016, **6**, 1–10.
12 I. Gabr and Tripathi and Prabhakar, A Coumarin-Benzothiazole Derivative as a FRET-Based Chemosensor of Adenosine 5′-Triphosphate, *Chemosensors*, 2019, **7**, 34.
13 X. Wan, C. Li, M. Zhang and Y. Chen, Acceptor–donor–acceptor type molecules for high performance organic photovoltaics – chemistry and mechanism, *Chem. Soc. Rev.*, 2020, **49**, 2828–2842.
14 E. Yalçin, Y. C. Kutlu, V. Korkmaz, E. Şahin and Z. Seferoğlu, 2,6-Dicyanoaniline based donor–acceptor compounds: the facile synthesis of fluorescent 3,5-diaryl/hetaryl-2,6-dicyanoanilines, *Arkivoc*, 2015, **2015**, 202–218.

15 M. Zheng, M. Sun, Y. Li, J. Wang, L. Bu, S. Xue and W. Yang, Piezofluorochromic properties of AIE-active 9,10-bis(*N*-alkylpheno-thiazin- 3-yl-vinyl-2)anthracenes with different length of alkyl chains, *Dyes Pigm.*, 2014, **102**, 29–34.

16 M. A. Shaheen, A. A. El-Emam and N. S. El-Gohary, 1,4,5,6,7,8-Hexahydroquinolines and 5,6,7,8-tetrahydronaphthalenes: a new class of antitumor agents targeting the colchicine binding site of tubulin, *Bioorg. Chem.*, 2020, **99**, 103831.

17 V. Anand and R. Dhamodharan, White light emission from fluorene-EDOT and phenothiazine-hydroquinone based D–π–A conjugated systems in solution, gel and film forms, *New J. Chem.*, 2017, **41**, 9741–9751.

18 B. Mohammadi, H. Kazemi and M. Shafieey, Simple pseudo-multicomponent synthesis of 2,6-dicyanoaniline derivatives *via* reaction between arylidenemalononitriles and malononitrile, *Monatsh. Chem.*, 2014, **145**, 1649–1652.

19 M. A. Pasha and B. Datta, Mechanochemistry: an efficient method of solvent-free synthesis of 3-amino-2,4-dicarbonitrile-5-methylbiphenyls, *J. Saudi Chem. Soc.*, 2014, **18**, 47–51.

20 J. R. Albani, New insights in the interpretation of tryptophan fluorescence: origin of the fluorescence lifetime and characterization of a new fluorescence parameter in proteins: the emission to excitation ratio, *J. Fluoresc.*, 2007, **17**, 406–417.

21 R. Kumaran and P. Ramamurthy, Denaturation mechanism of BSA by urea derivatives: evidence for hydrogen-bonding mode from fluorescence tools, *J. Fluoresc.*, 2011, **21**, 1499–1508.

22 S. J. Strickler and R. A. Berg, Relationship between absorption intensity and fluorescence lifetime of molecules, *J. Chem. Phys.*, 1962, **37**, 814–822.

23 T. Sen, K. K. Haldar and A. Patra, Au nanoparticle-based surface energy transfer probe for conformational changes of BSA protein, *J. Phys. Chem. C*, 2008, **112**, 17945–17951.

24 B. Valeur, *Mol. Fluoresc.*, 2012, 141–179.

25 C. Tahtaoui, F. Guillier, P. Klotz, J. L. Galzi, M. Hibert and B. Ilien, On the use of nonfluorescent dye labeled ligands in FRET-based receptor binding studies, *J. Med. Chem.*, 2005, **48**, 7847–7859.

26 S. Tyagi, S. A. E. Marras and F. R. Kramer, Wavelength-shifting molecular beacons, *Nat. Biotechnol.*, 2000, **18**, 1191–1196.

27 B. Dubertret, M. Calame and A. J. Libchaber, Single-mismatch detection using gold-quenched fluorescent oligonucleotid, *Nat. Biotechnol.*, 2001, **19**, 365–370.

28 S. A. E. Marras, F. R. Kramer and S. Tyagi, Efficiencies of fluorescence resonance energy transfer and contact-mediated quenching in oligonucleotide probes, *Nucleic Acids Res.*, 2002, **30**, 1–8.

29 R. Hovius, P. Vallotton, T. Wohland and H. Vogel, Fluorescence techniques: shedding light on ligand–receptor interactions, *Trends Pharmacol. Sci.*, 2000, **21**, 266–273.

30 M. K. Johansson, H. Fidder, D. Dick and R. M. Cook, Intramolecular dimers: a new strategy to flourescence quenching in dual-labeled oligonucleotide probes, *J. Am. Chem. Soc.*, 2002, **124**, 6950–6956.

31 I. L. Medintz, E. R. Goldman, M. E. Lassman and J. M. Mauro, A fluorescence resonance energy transfer sensor based on maltose binding protein, *Bioconjugate Chem.*, 2003, **14**, 909–918.

32 J. P. Knemeyer, N. Marmé and M. Sauer, Probes for detection of specific DNA sequences at the single-molecule level, *Anal. Chem.*, 2000, **72**, 3717–3724.

33 N. G. Walter and J. M. Burke, Real-time monitoring of hairpin ribozyme kinetics through base-specific quenching of fluorescein-labeled substrates, *RNA*, 1997, **4**, 392–404.

34 D. J. Maxwell, J. R. Taylor and S. Nie, Self-assembled nanoparticle probes for recognition and detection of biomolecules, *J. Am. Chem. Soc.*, 2002, **124**, 9606–9612.

35 J. R. Lakowicz, *Principles of fluorescence spectroscopy*, Kluwer Academic, New York, 1999.

36 M. K. Prashanth, M. Madaiah, H. D. Revanasiddappa and B. Veeresh, Synthesis, anticonvulsant, antioxidant and binding interaction of novel N-substituted methylquinazoline-2,4(1*H*,3*H*)-dione derivatives to bovine serum albumin: a structure-activity relationship study, *Spectrochim. Acta, Part A*, 2013, **110**, 324–332.

37 J. Mariam, P. M. Dongre and D. C. Kothari, Study of interaction of silver nanoparticles with bovine serum albumin using fluorescence spectroscopy, *J. Fluoresc.*, 2011, **21**, 2193–2199.

38 S. Bi, L. Ding, Y. Tian, D. Song, X. Zhou, X. Liu and H. Zhang, Investigation of the interaction between flavonoids and human serum albumin, *J. Mol. Struct.*, 2004, **703**, 37–45.

39 N. Dash, A. Mishra and G. Krishnamoorthy, Alkyl chain dependent interactions of ligands with bovine serum albumin, *J. Pharm. Biomed. Anal.*, 2013, **77**, 55–62.

40 T. Z. Janosi, J. Korppi-Tommola, Z. Csok, L. Kollar, P. Myllyperkio and J. Erostyak, Anthracene Fluorescence Quenching by a Tetrakis (Ketocarboxamide) Cavitand, *J. Spectrosc.*, 2014, **2014**, 708739.

41 C. Vijayakumar, V. K. Praveen, K. K. Kartha and A. Ajayaghosh, Excitation energy migration in oligo(*p*-phenylenevinylene) based organogels: Structure-property relationship and FRET efficiency, *Phys. Chem. Chem. Phys.*, 2011, **13**, 4942–4949.

42 F. Würthner, S. Ahmed, C. Thalacker and T. Debaerdemaeker, Core-substituted naphthalene bisimides: new fluorophors with tunable emission wavelength for FRET studies, *Chem.–Eur. J.*, 2002, **8**, 4742–4750.

43 B. Prusti and M. Chakravarty, An electron-rich small AIEgen as a solid platform for the selective and ultrasensitive on-site visual detection of TNT in the solid, solution and vapor states, *Analyst*, 2020, **145**, 1687–1694.

44 K. K. Karukstis, J. A. Fruetel and H. Terris, Multivariate analysis of Photosystem II fluorescence quenching by substituted benzoquinones and napthoquinones, *Biochim. Biophys. Acta*, 1987, **891**, 256–264.